Robotica: (2019) volume 37, pp. 1695–1709. © Cambridge University Press 2019
doi:10.1017/S0263574719000201

On the Cable Pseudo-Drag Problem of Cable-Driven Parallel Camera Robots at High Speeds

Huiling Wei†‡*, Yuanying Qiu‡* and Ying Sheng‡

†*College of Mechanical and Electrical Engineering, Foshan University, Foshan 528000, China*
‡*Key Laboratory of Ministry of Education for Electronic Equipment Structure Design, Xidian University, Xi'an 710071, China. E-mail: ysheng@xidian.edu.cn*

(Accepted January 29, 2019. First published online: March 4, 2019)

SUMMARY
This paper presents a control strategy for solving the cable pseudo-drag problem of cable-driven parallel camera robots at high speeds. The control strategy belongs to a hybrid position/tension control method based on cable tension optimization. The cable catenary model and cable pseudo-drag problem are considered firstly. Then, the dynamic model of the cable-driven parallel camera robot is established. The cable tension optimization is proposed. And then a control strategy is put forward and its stability is proved. Simulation results of a four-cable camera robot are presented and discussed.

KEYWORDS: Cable-driven parallel camera robot; Pseudo-drag; Cable tension optimization; Hybrid position/tension control; Stability analysis.

1. Introduction

With the advantages of large workspace, small inertia, simple structure, high speed, high mobility and so on, cable-driven parallel robots have become a hot research topic since the 1980s.[1]

Cable-driven parallel camera robots are a special kind of cable-driven parallel robots. Figure 1 shows a 5 m scale model of a cable-driven parallel camera robot in our laboratory at present. Speed control mode is adopted in this model. Because of the limited workspace of the model, it is only suitable to validate the principle of the control mode, and it cannot be used for high-speed experiments. It includes a mobile camera platform, four cables and four masts. The mobile camera platform is attached to the fixed pulleys through four cables, and the end-effector operates freely with three translational degrees of freedom in the workspace. A detailed explanation about three translational degrees of freedom is as follows:[2] The actual model in 3D space is of three translational degrees of freedom and three rotational degrees of freedom. But the camera robot consists of a translational mechanism and a second-stage rotating mechanism. The translation is implemented by four-cable traction, composite hinge structure and stable gyroscope. The composite hinge structure decouples the rotations and this paper can independently study the translation problems. The second-stage rotating mechanism is used to adjust the attitudes of the camera robot. Hence, the rotational degrees of freedom for the second-stage rotating mechanism can be uncoupled completely. So the camera platform in the workspace can be considered with three translational degrees of freedom, and it can be assumed to a point mass. Each pulley is attached to the top of the mast. The cables can be freely released by four servo motors arranged on the fixed bases, so that the camera platform can move freely in each direction. However, due to the unidirectional tension of the cable, the cable pseudo-drag problem becomes inevitable.[3–5] Especially when in high-speed motion and the vertical projection of the cable tension is

* Corresponding author. E-mails: weihuiling2007@126.com

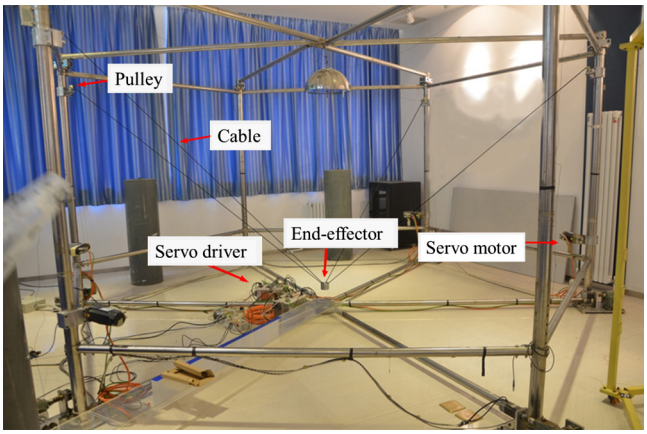

Fig. 1. Scale model of cable-driven parallel robots.

less than zero, the cable will suffer from the pseudo-drag problem such that the cable-driven parallel camera robot cannot work properly, leading to control system failure. Therefore, it is necessary to solve the cable pseudo-drag problem at high speeds.

Some researchers have discussed the cable pseudo-drag problem of cable-driven parallel robots. Wang et al.[6] proposed an optimization scheme for the cable tension configuration of the cable system according to the characteristics of the parallel macro–micro-robot suspension. The calculation shows that this optimization scheme makes the distribution of the cable tension more uniform and it avoids the cable pseudo-drag. The parallel macro–micro robot used in this method is scanned along a predetermined trajectory, and the cable tensions are optimized to ensure that the difference of the cable tensions is the smallest. That is to say, the uniformity of the cable tensions among the six suspensions is the best. But this method did not take the cable tension active control into consideration. Sun and Duan[7] discussed the cable pseudo-drag problem and gave the criterion of judgment; unfortunately there was not an effective method to solve the cable pseudo-drag problem. Tang et al.[8] proposed a new scheme of adding the liquid container structure on the moving platform of the cable-driven parallel cable robot to restrain the cable pseudo-drag. The working principle is by adding or reducing the liquid to change the location of the liquid centroid so as to change the cable tensions, thereby eliminating the cable pseudo-drag. For tons of heavy radio feed system, the mass of the liquid container can be ignored. However, adding the liquid container is not suitable for high-speed cable-driven parallel camera robots, since it will increase the mass of the cable-driven parallel camera robot, and the inertia cannot be ignored for the high-speed cable-driven parallel camera robots. Yao et al.[9] put forward a trajectory posture angle algorithm based on the force constraint function according to the characteristics of FAST feed support mechanism. The cable tension optimization algorithm of the cable-driven parallel mechanism can be obtained by analyzing the cable tension characteristics. This algorithm can optimize the attitude angles and the cable tensions of the feed support mechanism in the tracking process, guarantee the cable tension stably and smoothly and avoid the cable pseudo-drag effectively. However, this method is built on the established trajectory, while the movement trajectory of the high-speed cable-driven parallel camera robot is uncertain. Therefore, it is not suitable for high-speed cable-driven parallel camera robots. Tang and Shao[10] proposed a hybrid position/force control method for the FAST feed support system, which effectively prevents the cable pseudo-drag and realizes the precise attitude control. However, the working trajectory of the FAST feed support system is planned in advance, while that of the cable-driven parallel camera robots is constantly changing with the moving target. That is to say, the motion of the cable-driven parallel camera robot is in high mobility. More importantly, the tracking motion of the FAST feed support system is slow, while the motion of the cable-driven parallel camera robots is at high speeds. In addition, the work in ref. [10] does not optimize the cable tension and lacks the proof of the stability of the control strategy.

In our previous research work, aproportion-derivative(PD)-modified feedforward control strategy based on cable length feedback was used to track the trajectory and achieved a certain precision requirement, but the cable pseudo-drag problem arises at high speeds.[11] Hence, in order to solve the

https://doi.org/10.1017/S0263574719000201 Published online by Cambridge University Press

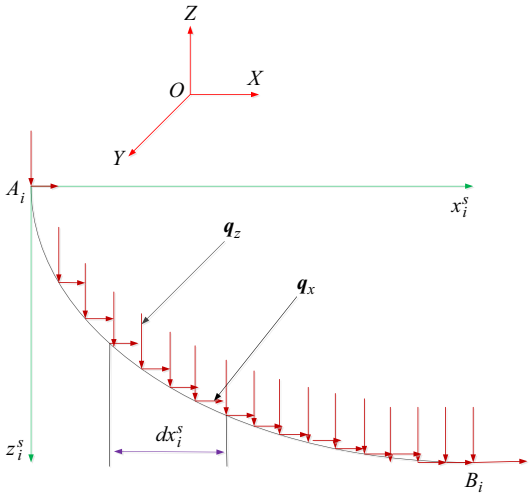

Fig. 2. Tension diagram of cable.

cable pseudo-drag problem at high speeds, this paper proposes an active synchronous tension control based on PD-modified feedforward control strategy. It is a hybrid position/tension control method that can achieve active tension control and avoid the cable pseudo-drag problem at high speeds. Firstly, we establish the catenary model of the cable-driven parallel camera robots to determine the critical condition of cable pseudo-drag in this paper. Then, a dynamic model is set up according to the catenary model, and the cable tensions are optimized. Furthermore, a hybrid position/tension control method based on cable tension optimization is designed and its stability is proved. Finally, the validity and rationality of the method are proved by simulation.

2. Description of Cable

2.1. Catenary model

It is necessary to take cable mass and span into consideration when the geometric dimension of a cable-driven parallel robot is relatively large. Therefore, the cable shape is described by the catenary model when the kinematic model is established.[12] In this case, it is more realistic to reflect the cable sag characteristics under the action of gravity, thus verifying the accuracy and authenticity of the kinematic model.

The speed and cable tension of each point on the cable are time varying in the catenary model. In order to establish the cable catenary model, we must know the position coordinates of each point on the cable. In order to simplify the theoretical model, the following assumptions are made in this paper:

(1) The connections among the cables, the frame and the end-effector are ideal.
(2) Cables meet ideal flexible condition: they cannot work in compression and in bend.
(3) The deformation of the cables conforms to Hooke's law.

A global fixed reference frame, noted by $\{O - XYZ\}$, is attached to the base of the cable-driven robot and is referred to as the base frame, where O is the origin point. Point A_i, at which the cable $i = 1, 2, \ldots, m$ is tangent to the pulley, is assumed to be fixed to the global fixed frame. The ith cable is attached at point B_i on the end-effector. A tension diagram of cable A_iB_i is shown in Fig. 2. The local coordinate system $\left\{A_i - x_i^s z_i^s\right\}$ in the vertical plane is established. A_i is the connection point between the ith cable and the pulley. B_i is the hinge point between the ith cable and the end-effector. $\boldsymbol{q}_x$ and $\boldsymbol{q}_z$ are the unit length loads of cable. Their directions are along the horizontal X-direction and vertical Z-direction, respectively.

The tension analysis of one cable span dx_i^s is shown in Fig. 3. Assuming $\boldsymbol{H}_i$ is the horizontal component of the cable tension for any point on the ith cable, the vertical component is $\boldsymbol{H}_i \frac{dz_i^s}{dx_i^s}$. When the end-effector is quasi-static, the static equilibrium condition of the cable differential unit is[13]

https://doi.org/10.1017/S0263574719000201 Published online by Cambridge University Press

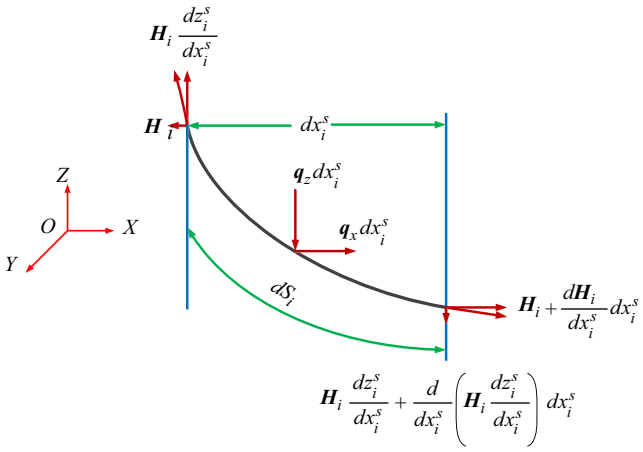

Fig. 3. Tension diagram of cable differential unit.

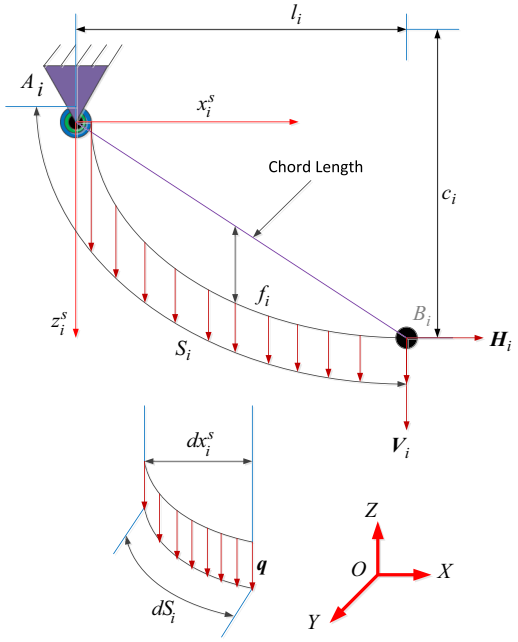

Fig. 4. Schematic diagram of a catenary model in the vertical plane.

$$\sum \boldsymbol{F}_{xi} = 0 \Rightarrow \frac{d\boldsymbol{H}_i}{dx_i^s} dx_i^s + \boldsymbol{q}_x dx_i^s = 0 \quad (i = 1, 2, \cdots, m) \tag{1}$$

$$\sum F_{zi} = 0 \Rightarrow \frac{d}{dx_i^s}\left(\boldsymbol{H}_i \frac{dz_i^s}{dx_i^s}\right) dx_i^s + \boldsymbol{q}_z dx_i^s = 0 \tag{2}$$

Suppose the cables that are only subjected to their own gravity. The load of the X-direction is zero. From Eq. (1), $\frac{d\boldsymbol{H}_i}{dx_i^s} dx_i^s = 0$ holds. Eq. (2) can be further arranged as:[13]

$$\boldsymbol{H}_i \frac{d^2 z_i^s}{d\left(x_i^s\right)^2} + \boldsymbol{q}_z = 0 \tag{3}$$

The effects of the cable sags on the dynamics must be considered in large-span cables,[14] leading to a cable catenary model.

The local coordinate system $\left\{A_i - x_i^s z_i^s\right\}$ in the vertical plane is established as shown in Fig. 4. Point A_i is the local coordinate origin. $\boldsymbol{H}_i$ is the horizontal component of the cable tension of the ith

https://doi.org/10.1017/S0263574719000201 Published online by Cambridge University Press

cable, $\boldsymbol{V}_i$ is the vertical component of the cable tension of the ith cable, l_i is the horizontal span of the ith cable, c_i is the vertical span of the ith cable, f_i is the mid-span sag of the ith cable and S_i is the ith cable length.

$\boldsymbol{q}$ is the uniform load along the cable length under its own gravity, which can be expressed as:[15]

$$\boldsymbol{q}dS_i = \boldsymbol{q}_z dx_i^s \tag{4}$$

where $\boldsymbol{q} = \rho \boldsymbol{g}$. ρ is the linear density of the cable; $\boldsymbol{g} = 9.8\ \mathrm{m/s^2}$ is the gravity acceleration.

According to the arc length formula, one can obtain:[13]

$$\boldsymbol{q}_z = \boldsymbol{q}\frac{dS_i}{dx_i^s} = \boldsymbol{q}\sqrt{1+\left(\frac{dz_i^s}{dx_i^s}\right)^2} \tag{5}$$

Substituting Eq. (5) into Eq. (3), one can obtain

$$\boldsymbol{H}_i \frac{d^2 z_i^s}{d\left(x_i^s\right)^2} + \boldsymbol{q}\sqrt{1+\left(\frac{dz_i^s}{dx_i^s}\right)^2} = 0 \tag{6}$$

Upon rearranging Eq. (6), the solution to the boundary conditions shown in Fig. 4 is obtained. It is[15]

$$z_i^s = \frac{\boldsymbol{H}_i}{\boldsymbol{q}}\left[\cosh\alpha_i - \cosh\left(\frac{2\beta_i x_i^s}{l_i} - \alpha_i\right)\right] \tag{7}$$

where $\alpha_i = \sinh^{-1}\left[\frac{\beta_i(c_i/l_i)}{\sinh\beta_i}\right] + \beta_i$, $\beta_i = \frac{\boldsymbol{q}l_i}{2\boldsymbol{H}_i}$.

Eq. (7) represents a catenary in mathematics. It describes the shape of a cable under the action of gravity. By considering the coordinates of any point on the curve, the entire curve can be completely determined.

According to the formula derivation, the cable length is given by[15]

$$S_i = \int_0^{l_i}\sqrt{1+\left(\frac{dz_i^s}{dx_i^s}\right)^2}dx_i^s = l_i + \frac{\boldsymbol{H}_i\left(e^{2\alpha_i}+e^{4\beta_i}\right)\left(e^{2\alpha_i}-e^{4\beta_i}\right)}{16\rho\boldsymbol{g}e^{4\beta_i+2\alpha_i}} - \frac{\boldsymbol{H}_i}{2} \tag{8}$$

When $x_i^s = l_i/2$, the mid-span sag of the cable can be obtained from[15]

$$f_i = \frac{8\boldsymbol{H}_i\sinh\beta_i\sinh^{-1}\left(\frac{\rho\boldsymbol{g}c_i/2\boldsymbol{H}_i}{\sinh\beta_i}\right) - c_i\rho\boldsymbol{g}}{2\rho\boldsymbol{g}} \tag{9}$$

2.2. *Pseudo-drag problem*

Assume that γ_0 and γ_i are the azimuth angles of cable tension $\boldsymbol{T}_0$ and $\boldsymbol{T}_i$ at $(0, 0)$ and (l_i, c_i), respectively. We have

$$\begin{cases}\tan\gamma_0 = -\dfrac{\boldsymbol{V}_0}{\boldsymbol{H}_0}\\ \tan\gamma_i = \dfrac{\boldsymbol{V}_i}{\boldsymbol{H}_i}\end{cases} \tag{10}$$

where, $\boldsymbol{V}_0$ and $\boldsymbol{V}_i$ are the vertical components of cable tension of the catenary at $(0, 0)$ and (l_i, c_i), respectively. They satisfy the following relationship:

$$\boldsymbol{V}_0 = \boldsymbol{V}_i + \rho\boldsymbol{g}S_i \tag{11}$$

According to previous studies,[6,7] when l_i, c_i are constant, according to $\boldsymbol{V}_i$ we can analyze the three states of the cable:

(a) When $\boldsymbol{V}_i = 0$, according to Eq. (10), we have $\tan\gamma_i = \frac{\boldsymbol{V}_i}{\boldsymbol{H}_i} = 0$. The state of the cable is shown in Fig. 5(a), where the cable is in a critical state.

https://doi.org/10.1017/S0263574719000201 Published online by Cambridge University Press

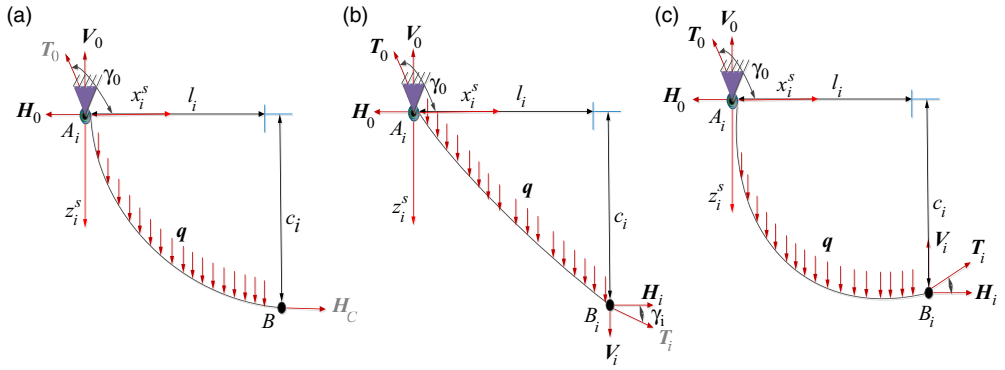

Fig. 5. Three states of cable tensions, (a) $\boldsymbol{V}_i = 0$, (b) $\boldsymbol{V}_i > 0$, and (c) $\boldsymbol{V}_i < 0$.

(b) When $\boldsymbol{V}_i > 0$, according to Eq. (10), we have $\tan \gamma_i = \frac{\boldsymbol{V}_i}{\boldsymbol{H}_i} > 0$. The state of the cable is shown in Fig. 5(b), where the cable is in a tight state.
(c) When $\boldsymbol{V}_i < 0$, according to Eq. (10), we have $\tan \gamma_i = \frac{\boldsymbol{V}_i}{\boldsymbol{H}_i} < 0$. The state of the cable is shown in Fig. 5(c), where the cable is in the pseudo-drag state.

As we all know that if a cable is in the pseudo-drag state, it means that other cables not only withstand their own weights and the system weight, but also bear the extra load from the pseudo-drag cable. This situation will lead to uneven tensions. Because the cable-driven parallel robots have a real hysteresis in control, when the cable tension is smaller, the cable stiffness will be smaller, and thus the real hysteresis is more obvious. Hence, when the consistency of the cable tension is bad, the difference of the time delay of cable will be large and the control consistency will be poor such that the cable-driven parallel robots cannot work properly, leading to control system failure. As a result, the cable-driven parallel robots should avoid the cable pseudo-drag problem as much as possible.

According to the above analysis, we know that the cable-driven parallel robots work properly when $\boldsymbol{V}_i \geq 0$. On the contrary, the cable-driven parallel robots are in the pseudo-drag state when $\boldsymbol{V}_i < 0$; therefore, in order to avoid the cable pseudo-drag problem, we should increase $\boldsymbol{V}_i$ at this moment.

3. System Dynamics Model

The cables and the end-effector are regarded as a research unit. Hence, the dynamics of the research unit in the global coordinate can be written as follows:[11,16]

$$\boldsymbol{M}(\boldsymbol{X})\ddot{\boldsymbol{X}} + \boldsymbol{N}\left(\boldsymbol{X}, \dot{\boldsymbol{X}}\right)\dot{\boldsymbol{X}} + \boldsymbol{P}(\boldsymbol{X})\,\boldsymbol{M}_c + \boldsymbol{F}_g + \boldsymbol{W}_g - \boldsymbol{W}_e = \boldsymbol{J}\boldsymbol{H} \tag{12}$$

where, $\boldsymbol{M}(\boldsymbol{X})$ is the mass-related item; $\ddot{\boldsymbol{X}}$ is the generalized acceleration of the end-effector; $\boldsymbol{N}\left(\boldsymbol{X}, \dot{\boldsymbol{X}}\right)$ is the speed-related item; $\dot{\boldsymbol{X}}$ is the generalized speed of the end-effector; $\boldsymbol{P}(\boldsymbol{X})$ is the cable inertia-related item; $\boldsymbol{M}_c$ is the cable mass; $\boldsymbol{F}_g$ is the gravitational force of the cable-related item; $\boldsymbol{W}_g$ is the gravitational force of the end-effector; $\boldsymbol{W}_e$ is the generalized external force exerted on the end-effector center point by the environment; $\boldsymbol{H}$ is the vector describing horizontal components of all the cable tensions; and $\boldsymbol{J}$ is a Jacobian matrix, $\boldsymbol{J} = \begin{bmatrix} {}^o\boldsymbol{u}_1 & \cdots & {}^o\boldsymbol{u}_m \\ ({}^o\mathfrak{R}_p\,{}^p\boldsymbol{B}_1) \times {}^o\boldsymbol{u}_1 & \cdots & ({}^o\mathfrak{R}_p\,{}^p\boldsymbol{B}_m) \times {}^o\boldsymbol{u}_m \end{bmatrix} \in \boldsymbol{R}^{n\times m}$, ${}^o\boldsymbol{u}_i = \begin{bmatrix} \cos\theta_i & \sin\theta_i & \tan\gamma_i \end{bmatrix}^T$ is along the tangential direction of the ith cable tension $\boldsymbol{T}_i$ at the end node B_i.

On simplifying, Eq. (12) becomes

$$\boldsymbol{J}\boldsymbol{H} = \boldsymbol{Q} \tag{13}$$

Considering the actuator dynamics formulated as $\boldsymbol{\tau} = \boldsymbol{A}\ddot{\boldsymbol{\varphi}} + \boldsymbol{C}\dot{\boldsymbol{\varphi}} + \boldsymbol{r}\boldsymbol{T}$, and $\boldsymbol{T} = \boldsymbol{H}\sqrt{1 + \tan^2\gamma}$, we obtain the system dynamics model:

$$\boldsymbol{M}_{eq}(\boldsymbol{X})\,\ddot{\boldsymbol{X}} + \boldsymbol{N}_{eq}\left(\boldsymbol{X}, \dot{\boldsymbol{X}}\right)\dot{\boldsymbol{X}}\boldsymbol{G}_{eq}(\boldsymbol{X}) = \boldsymbol{J}^T\boldsymbol{\tau} \tag{14}$$

https://doi.org/10.1017/S0263574719000201 Published online by Cambridge University Press

where

$$\begin{cases} \boldsymbol{M}_{eq}(\boldsymbol{X}) = \boldsymbol{r}\sqrt{1+\tan^2\gamma}\boldsymbol{M}(\boldsymbol{X}) + \boldsymbol{r}^{-1}\boldsymbol{J}^T\boldsymbol{A}\boldsymbol{J} \\ \boldsymbol{N}_{eq}\left(\boldsymbol{X},\dot{\boldsymbol{X}}\right) = \boldsymbol{r}\sqrt{1+\tan^2\gamma}\boldsymbol{N}\left(\boldsymbol{X},\dot{\boldsymbol{X}}\right) + \boldsymbol{r}^{-1}\boldsymbol{J}^T\boldsymbol{A}\dot{\boldsymbol{J}}\boldsymbol{r}^{-1}\boldsymbol{J}^T\boldsymbol{C}\boldsymbol{J}\dot{\boldsymbol{X}} \\ \boldsymbol{G}_{eq}(\boldsymbol{X}) = \boldsymbol{r}\sqrt{1+\tan^2\gamma}\boldsymbol{P}(\boldsymbol{X})\,\boldsymbol{M}_c + \boldsymbol{r}\sqrt{1+\tan^2\gamma}\left(\boldsymbol{F}_g + \boldsymbol{W}_g - \boldsymbol{W}_e\right) \end{cases} \tag{15}$$

where, $\boldsymbol{\tau}$ is the torque of the motors; $\boldsymbol{r}$ is the vector of the winch radius; $\boldsymbol{A}$ is the inertia matrix; and $\boldsymbol{C}$ is the viscous friction coefficient of the motors.

4. Cable Tension Optimization

In order to ensure the end-effector to be completely controllable, it is necessary to carry out redundant actuation for the cable-driven parallel camera robots.[17] According to the kinematics equation, there are more than one solution set of the cable tensions when the trajectories of the end-effector are known. However, we need to obtain the real-time tension of each cable in the actual motion control. Therefore, it is necessary to optimize the distribution of the cable tensions to get a unique solution.

The fully constrained cable-driven parallel camera robot is a highly coupled nonlinear system, and it is also a redundant drive system. Hence, we need to solve the uncertainty of the cable tensions by optimizing the distribution of the cable tensions when designing the control scheme. In this paper, we choose the minimum variance as the optimization target of the cable tensions, and then a set of unique tension solutions is obtained.[16]

By introducing the Moore–Penrose generalized inverse $\boldsymbol{J}^{\dagger}$ of the structure matrix $\boldsymbol{J}$, the horizontal component of the cable tension is obtained according to Eq. (12):[16,18]

$$\boldsymbol{H} = \boldsymbol{H}_{\mathrm{s}} + \boldsymbol{H}_{\mathrm{h}} \tag{16}$$

where $\boldsymbol{H}_{\mathrm{s}}$ is the special solution set of the cable tensions and $\boldsymbol{H}_{\mathrm{h}}$ is the general solution set of the cable tensions. The special solution set and the general solution set can be obtained by the following formulas:

$$\boldsymbol{H}_{\mathrm{s}} = \left[H_{\mathrm{s}}^1,\ H_{\mathrm{s}}^2, \ldots, H_{\mathrm{s}}^m\right]^T \boldsymbol{J}^{+}\boldsymbol{Q} \tag{17}$$

$$\boldsymbol{H}_{\mathrm{h}} = \boldsymbol{N}(\boldsymbol{J})\,\lambda \tag{18}$$

where $\boldsymbol{N}(\boldsymbol{J}) = \left[\boldsymbol{N}_1, \boldsymbol{N}_2, \cdots, \boldsymbol{N}_{m-n}\right] \in \mathbf{R}^{m\times(m-n)}$ is the zero space matrix of the structure matrix $\boldsymbol{J}$; $\boldsymbol{N}_1, \boldsymbol{N}_2, \ldots, \boldsymbol{N}_m$ are the m-dimensional column vectors; and $\lambda \in \mathbf{R}^{(m-n)\times 1}$ is the $(m\text{-}n)$ dimensional column vector, known as the tension coefficient. As shown in Fig. 4, the vertical component $\boldsymbol{V}_i$ of the cable tension at point B_i is obtained:

$$\boldsymbol{V}_i = \boldsymbol{H}_i \tan\gamma_i \ (i = 1, 2, \ldots, m) \tag{19}$$

The cable tension $\boldsymbol{T}_i$ at point B_i is obtained by the following formula:

$$\boldsymbol{T}_i = \boldsymbol{H}_i\sqrt{1+\tan^2\gamma_i} \ (i = 1, 2, \ldots, m) \tag{20}$$

In order to ensure the cable-driven parallel camera robots can work normally, the cable tension $\boldsymbol{T}_i$ must meet the following conditions:

$$0 \le \boldsymbol{T}_{\min} \le \boldsymbol{T}_i \le \boldsymbol{T}_{\max} \tag{21}$$

where, the lower limit $\boldsymbol{T}_{\min}$ of the cable tensions ensures the cables are tensioned, while the upper limit $\boldsymbol{T}_{\max}$ of the cable tensions is determined by the output torque of the servo motor and the maximum breaking tension of the cable.

In order to make the cable-driven parallel camera robots work steadily, the difference among the cable tensions should be as small as possible. Hence, it is necessary to design a reasonable distribution of the cable tensions. The minimum variance is used as the optimization target of the cable tensions in this paper. According to the work in ref. [16], the minimum variance as the optimization target can satisfy the real time and continuity requirements of the cable tensions. Equations (12) and (20) are used as constraint conditions, and the problem for solving the cable tension transforms into

https://doi.org/10.1017/S0263574719000201 Published online by Cambridge University Press

a constraint optimization problem. The mathematical expression of the constraint optimization can be written as follows:

$$\begin{aligned} &\text{Objective} \qquad F(\lambda) = \min \left(\frac{1}{m} \left[\sum_{i=1}^{m} (\boldsymbol{H}_{\mathrm{i}} - E(\boldsymbol{H}))^2 \right] \right) \\ &\text{Constraint} \qquad \boldsymbol{JH} = \boldsymbol{Q} \\ &\qquad\qquad 0 \le \boldsymbol{T}_{\min} \le \boldsymbol{T}_i \le \boldsymbol{T}_{\max} \end{aligned} \tag{22}$$

where $\boldsymbol{H}_i = \boldsymbol{H}_{\mathrm{s}}^i + \widehat{\boldsymbol{N}}(\mathrm{J})_i \lambda$, $E(\boldsymbol{H}) = \frac{\sum_{i=1}^{m} \left(\boldsymbol{H}_{\mathrm{s}}^i + \widehat{\boldsymbol{N}}(\boldsymbol{J})_i \lambda \right)}{m}$, and $\widehat{\boldsymbol{N}}(\boldsymbol{J})_i$ is the ith row of the zero-space matrix $N(J)$A. λ is a 4×3-dimensional column vector.

5. Hybrid Position/Tension Control Based on Cable Tension Optimization

In order to achieve high precision and stable tracking task in continuous rapid motion of the cable-driven parallel camera robots, it is necessary to design a stable, reasonable and effective control strategy. Therefore, we present a hybrid position/tension control method in this paper. It is based on the dynamics model of the cable-driven parallel camera robot and the cable tension optimization. Also, the hybrid controller includes a PD-modified feedforward controller based on the dynamic model of the cable-driven parallel camera robots and an active synchronous cable tension controller based on the catenary kinematics model. The role of the PD-modified feedforward controller is to ensure the accuracy of position tracking. The purpose of the active synchronous cable tension controller is to ensure the tensioning of cables in real time.

The cable pseudo-drag problem arises in continuous rapid motion for the cable-driven camera robots, and therefore, the active synchronous control of the cable tensions is necessary. There is a cable pseudo-drag phenomenon when the vertical cable tension is less than zero for a large-span cable-driven parallel robot. In this case, the cable tensions increase via tightening the cable length, at the same time releasing the cable length. That is to say, the cable tension and the cable length are coupled within a certain range. Hence, the cable tension can be controlled by adjusting the cable length. This is the main idea of active synchronous cable tension control.

Therefore, the active synchronous cable tension control is applied based on the closed loop position control in this paper, which not only satisfies the high precision position tracking at high speeds, but also avoids the cable pseudo-drag problem.

5.1. Control strategy

The hybrid position/tension control method based on the cable tension optimization is shown in Fig. 6. One is the position control loop and the other is the active synchronous cable tension control loop. The purpose of the position control loop is to ensure the accurate tracking of the end-effector. The purpose of the active synchronous cable tension control loop is to avoid the cable pseudo-drag in the high-speed motion state. The end-effector position is controlled by the position error signal, and the cable tensions are controlled by the cable length signals.

As shown in Fig. 6, there are two forms of cable length adjustments: form A and form B. The purpose of form A is to adjust the cable lengths after optimal distribution of cable tensions, and the purpose of form B is to inhibit the cable pseudo-drag. The cable tensions and the cable lengths are coupled in a certain range for the cable-driven parallel robots. The problem of cable pseudo-drag arises when the actual vertical cable tension is less than zero; at this situation, the active synchronous cable tension controller is required to tighten the pseudo-drag cable. The tension control for a pseudo-drag cable from the active synchronous is in the form of cable length adjustment, and it is superimposed into the PD-modified feedforward controller, as shown in Fig. 6. The position error between the actual position and the desired position is real-time feedforward, as shown in Fig. 6.

The control law of the hybrid controller is as follows:

$$\boldsymbol{\tau} = \boldsymbol{\tau}_1 + \boldsymbol{\tau}_3 \tag{23}$$

where $\boldsymbol{\tau}_1$ is the PD-modified feedforward control law and $\boldsymbol{\tau}_3$ is the active synchronous cable tension control law.

https://doi.org/10.1017/S0263574719000201 Published online by Cambridge University Press

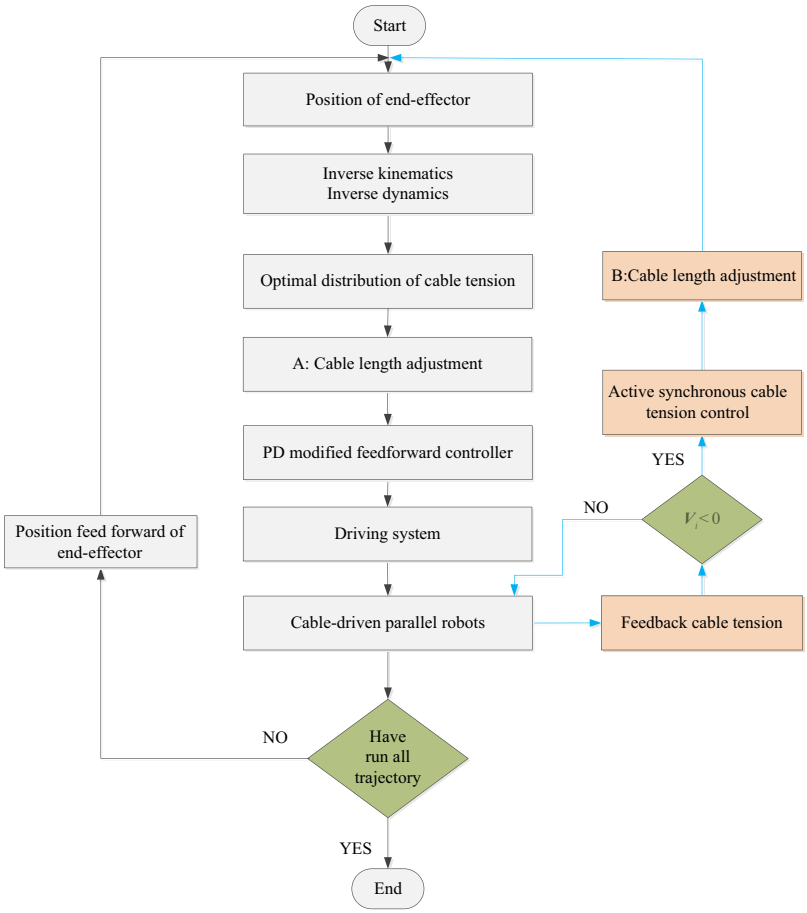

Fig. 6. Schematic diagram of hybrid position/tension control.

Suppose the desired position is $\boldsymbol{X}_d$, the PD-modified feedforward control law is given as:

$$\boldsymbol{\tau}_1 = \boldsymbol{J}^{\dagger}\left(\boldsymbol{M}_{eq}\left(\boldsymbol{X}\right)\ddot{\boldsymbol{X}}_d + \boldsymbol{N}_{eq}\left(\boldsymbol{X},\dot{\boldsymbol{X}}\right)\dot{\boldsymbol{X}}_d + \boldsymbol{G}_{eq}\left(\boldsymbol{X}\right) + \boldsymbol{K}_{pp}\left(\boldsymbol{X}_d - \boldsymbol{X}\right) + \boldsymbol{K}_{pd}\left(\dot{\boldsymbol{X}}_d - \dot{\boldsymbol{X}}\right)\right) \tag{24}$$

where, $\boldsymbol{K}_{pp}$ and $\boldsymbol{K}_{pd}$ are the feedback gain matrixes of the positions; $\boldsymbol{J}^{\dagger}$ denotes the generalized inverse of $\boldsymbol{J}^T$, $\boldsymbol{J}^{\dagger}\boldsymbol{J}\left(\boldsymbol{J}^T\boldsymbol{J}\right)^{-1}$; and $\boldsymbol{e} = \boldsymbol{X}_d - \boldsymbol{X}$ is the position error.

The output of the active synchronous cable tension controller is based on the cable length adjustment corresponding to the cable tension difference $\boldsymbol{H} - \boldsymbol{H}_d$. The cable tension difference comes from the actual cable tension and the maximum adjusted cable tension of the PD controller. Using PD logic control, its control law is as follows:

$$\boldsymbol{\tau}_3 = \boldsymbol{K}_{lp}\left(l_d - l\right) + \boldsymbol{K}_{ld}\left(\dot{l}_d - \dot{l}\right) \tag{25}$$

where $\boldsymbol{K}_{lp}$ and $\boldsymbol{K}_{ld}$ are the feedback gain matrixes of the cable lengths and $\boldsymbol{e}_l = l_d - l$ is the cable length error.

Substituting Eqs. (23)–(25) into Eq. (14), we have:

$$\begin{aligned}
&\boldsymbol{M}_{eq}\left(\boldsymbol{X}\right)\ddot{\boldsymbol{X}} + \boldsymbol{N}_{eq}\left(\boldsymbol{X},\dot{\boldsymbol{X}}\right)\dot{\boldsymbol{X}} + \boldsymbol{G}_{eq}\left(\boldsymbol{X}\right) = \boldsymbol{J}^T\left(\boldsymbol{\tau}_1 + \boldsymbol{\tau}_3\right)\\
&\boldsymbol{M}_{eq}\left(\boldsymbol{X}\right)\ddot{\boldsymbol{X}} - \boldsymbol{M}_{eq}\left(\boldsymbol{X}\right)\ddot{\boldsymbol{X}}_d + \boldsymbol{N}_{eq}\left(\boldsymbol{X},\dot{\boldsymbol{X}}\right)\dot{\boldsymbol{X}} - \boldsymbol{N}_{eq}\left(\boldsymbol{X},\dot{\boldsymbol{X}}\right)\dot{\boldsymbol{X}}_d - \boldsymbol{K}_{pp}\boldsymbol{e} - \boldsymbol{K}_{pd}\dot{\boldsymbol{e}} - \boldsymbol{J}^T\boldsymbol{K}_{lp}\boldsymbol{e}_l - \boldsymbol{J}^T\boldsymbol{K}_{ld}\dot{\boldsymbol{e}}_l = 0\\
&\boldsymbol{M}_{eq}\left(\boldsymbol{X}\right)\ddot{\boldsymbol{e}} + \boldsymbol{N}_{eq}\left(\boldsymbol{X},\dot{\boldsymbol{X}}\right)\dot{\boldsymbol{e}} + \boldsymbol{K}_{pp}\boldsymbol{e} + \boldsymbol{K}_{pd}\dot{\boldsymbol{e}} + \boldsymbol{J}^T\boldsymbol{K}_{lp}\boldsymbol{e}_l + \boldsymbol{J}^T\boldsymbol{K}_{ld}\dot{\boldsymbol{e}}_l = 0
\end{aligned} \tag{26}$$

5.2. Stability analysis

In order to prove the stability of the control strategy, we should build the Lyapunov scalar function of Eq. (26) firstly. According to the system energy, the Lyapunov scalar function is established as follows:

https://doi.org/10.1017/S0263574719000201 Published online by Cambridge University Press

$$V = \frac{1}{2}\dot{\boldsymbol{e}}^T \boldsymbol{M}_{eq}(\boldsymbol{X})\,\dot{\boldsymbol{e}} + \frac{1}{2}\boldsymbol{e}^T \boldsymbol{K}_{pp}\boldsymbol{e} + \frac{1}{2}\boldsymbol{e}_l^T \boldsymbol{K}_{lp}\boldsymbol{e}_l \tag{27}$$

According to Eq. (27), one obtains the derivative of Lyapunov scalar function:

$$\dot{V} = \dot{\boldsymbol{e}}^T \boldsymbol{M}_{eq}(\boldsymbol{X})\,\ddot{\boldsymbol{e}} + \frac{1}{2}\dot{\boldsymbol{e}}^T \dot{\boldsymbol{M}}_{eq}(\boldsymbol{X})\,\dot{\boldsymbol{e}} + \dot{\boldsymbol{e}}^T \boldsymbol{K}_{pp}\boldsymbol{e} + \dot{\boldsymbol{e}}_l^T \boldsymbol{K}_{lp}\boldsymbol{e}_l \tag{28}$$

Substituting Eq. (26) into Eq. (28), we have:

$$\begin{aligned}\dot{V} &= \dot{\boldsymbol{e}}^T \boldsymbol{M}_{eq}(\boldsymbol{X})\,\ddot{\boldsymbol{e}} + \frac{1}{2}\dot{\boldsymbol{e}}^T \dot{\boldsymbol{M}}_{eq}(\boldsymbol{X})\,\dot{\boldsymbol{e}} + \dot{\boldsymbol{e}}^T \boldsymbol{K}_{pp}\boldsymbol{e} + \dot{\boldsymbol{e}}_l^T \boldsymbol{K}_{lp}\boldsymbol{e}_l \\ &= \dot{\boldsymbol{e}}^T \left(\frac{1}{2}\dot{\boldsymbol{M}}_{eq}(\boldsymbol{X}) - \boldsymbol{N}_{eq}(\boldsymbol{X},\dot{\boldsymbol{X}})\right)\dot{\boldsymbol{e}} - \dot{\boldsymbol{e}}^T \boldsymbol{K}_{pd}\dot{\boldsymbol{e}} - \dot{\boldsymbol{e}}^T \boldsymbol{J}^T \boldsymbol{K}_{lp}\boldsymbol{e}_l - \dot{\boldsymbol{e}}^T \boldsymbol{J}^T \boldsymbol{K}_{ld}\dot{\boldsymbol{e}}_l + \dot{\boldsymbol{e}}_l^T \boldsymbol{K}_{lp}\boldsymbol{e}_l\end{aligned} \tag{29}$$

According to the mapping relations $\boldsymbol{e}_l = -\boldsymbol{J}^T\boldsymbol{e}$ between the change of the end-effector position and the change of the cable length, we have:

$$\begin{aligned}\dot{V} &= \dot{\boldsymbol{e}}^T \left(\frac{1}{2}\dot{\boldsymbol{M}}_{eq}(\boldsymbol{X}) - \boldsymbol{N}_{eq}(\boldsymbol{X},\dot{\boldsymbol{X}})\right)\dot{\boldsymbol{e}} - \dot{\boldsymbol{e}}^T \boldsymbol{K}_{pd}\dot{\boldsymbol{e}} - \dot{\boldsymbol{e}}^T \boldsymbol{J}^T \boldsymbol{K}_{lp}\boldsymbol{e}_l - \dot{\boldsymbol{e}}^T \boldsymbol{J}^T \boldsymbol{K}_{ld}\dot{\boldsymbol{e}}_l + \dot{\boldsymbol{e}}_l^T \boldsymbol{K}_{lp}\boldsymbol{e}_l \\ &= \dot{\boldsymbol{e}}^T \left(\frac{1}{2}\dot{\boldsymbol{M}}_{eq}(\boldsymbol{X}) - \boldsymbol{N}_{eq}(\boldsymbol{X},\dot{\boldsymbol{X}})\right)\dot{\boldsymbol{e}} - \dot{\boldsymbol{e}}^T \boldsymbol{K}_{pd}\dot{\boldsymbol{e}} - \dot{\boldsymbol{e}}^T \boldsymbol{J}^T \boldsymbol{K}_{lp}\boldsymbol{e}_l - \dot{\boldsymbol{e}}^T \boldsymbol{J}^T \boldsymbol{K}_{ld}\boldsymbol{J}\dot{\boldsymbol{e}} + \dot{\boldsymbol{e}}^T \boldsymbol{J}^T \boldsymbol{K}_{lp}\boldsymbol{e}_l \\ &= \dot{\boldsymbol{e}}^T \left(\frac{1}{2}\dot{\boldsymbol{M}}_{eq}(\boldsymbol{X}) - \boldsymbol{N}_{eq}(\boldsymbol{X},\dot{\boldsymbol{X}})\right)\dot{\boldsymbol{e}} - \dot{\boldsymbol{e}}^T \left(\boldsymbol{K}_{pd} + \boldsymbol{J}^T \boldsymbol{K}_{ld}\boldsymbol{J}\right)\dot{\boldsymbol{e}}\end{aligned} \tag{30}$$

According to the robot dynamics, the nonlinear robot system has the structural characteristics $\dot{\boldsymbol{e}}^T\left(\frac{1}{2}\dot{\boldsymbol{M}}_{eq}(\boldsymbol{X}) - \boldsymbol{N}_{eq}(\boldsymbol{X},\dot{\boldsymbol{X}})\right)\dot{\boldsymbol{e}} = 0$.[19] Hence, Eq. (30) can be simplified as:

$$\dot{V} = -\dot{\boldsymbol{e}}^T \left(\boldsymbol{K}_{pd} + \boldsymbol{J}^T \boldsymbol{K}_{ld}\boldsymbol{J}\right)\dot{\boldsymbol{e}} \tag{31}$$

where $\boldsymbol{K}_{ld}$ is a positive definite matrix. Thus $\boldsymbol{J}^T\boldsymbol{K}_{ld}\boldsymbol{J}$ is also a positive definite matrix and satisfies the following relation:[20]

$$y^T\left(\boldsymbol{J}^T\boldsymbol{K}_{ld}\boldsymbol{J}\right)y = y^T\left(\boldsymbol{J}^T\boldsymbol{K}_{ld}^{\frac{1}{2}}\boldsymbol{K}_{ld}^{\frac{1}{2}}\boldsymbol{J}\right)y = z^T z > 0 \tag{32}$$

where z is an arbitrary nonzero vector.

The sum $\left(\boldsymbol{K}_{pd} + \boldsymbol{J}^T\boldsymbol{K}_{ld}\boldsymbol{J}\right)$ of the two PD matrices is still a PD matrix. Hence, we get the conclusion as follows:

$$\dot{V} \le 0 \tag{33}$$

Thus, the motion under the control strategy converges to the maximum invariant set satisfying $\dot{V} = 0$. At this point, there is $\dot{e} = 0$. According to Eq. (25), we have the maximum invariant set as follows:

$$\left(\boldsymbol{K}_{pd} + \boldsymbol{J}^T\boldsymbol{K}_{ld}\boldsymbol{J}\right)\boldsymbol{e} = 0 \tag{34}$$

Since $\left(\boldsymbol{K}_{pd} + \boldsymbol{J}^T\boldsymbol{K}_{ld}\boldsymbol{J}\right)$ is a positive definite matrix, there is $\boldsymbol{e} = 0$. Hence, we get the conclusion that when $t \to \infty$ there is $\boldsymbol{X} \to \boldsymbol{X}_d$ in the workspace. That is to say, the motion is carried out as expected and the system is stable.

6. Numerical Simulation

6.1. Description of the parameters

In order to prove the effectiveness of the control strategy, this paper uses a cable-driven parallel camera robot with three translational degrees of freedom in the workspace to design the simulation experiments. And the simulation experiments are done by using MATLAB.

https://doi.org/10.1017/S0263574719000201 Published online by Cambridge University Press

Table I. Simulation parameters of camera robot.

Item	Symbol	Value
End-effector mass	m	20 kg
Position of 1# pulley	A_1	$\begin{bmatrix}-100 & 50 & 25\end{bmatrix}^T$ m
Position of 2# pulley	A_2	$\begin{bmatrix}100 & 50 & 25\end{bmatrix}^T$ m
Position of 3# pulley	A_3	$\begin{bmatrix}100 & -50 & 25\end{bmatrix}^T$ m
Position of 4# pulley	A_4	$\begin{bmatrix}-100 & -50 & 25\end{bmatrix}^T$ m
Elastic modulus of cable	E	2.8×10^4 MPa
Nominal diameter of cable	d	3 mm
Mass of unit cable length	m_0	0.0456 kg/m
Upper bound of cable tension	$\boldsymbol{T}_{\max}$	3000 N
Lower bound of cable tension	$\boldsymbol{T}_{\min}$	10 N
Viscous damping coefficient of cable	c	$0.2\ \mathrm{N \cdot s/m}$
Upper bound of motor rated output torque	$\boldsymbol{\tau}_{\max}$	$15.8\ \mathrm{N \cdot m}$
Rotational inertia of motor	$\boldsymbol{A}$	$7.52 \times 10^{-4}\ \mathrm{kg \cdot m^2}$
Viscous damping coefficient of motor	$\boldsymbol{C}$	$1.88 \times 10^{-4}\ \mathrm{N \cdot s/m}$
Reduction ratio of motor	n	4 : 1
The radius of winch	$r_{w,i}$	0.04 m

The cable-driven parallel camera robot model in this paper is based on a 200×100 m model. Choosing the site center as the origin of the global coordinate system, the simulation parameters of the cable-driven parallel camera robot are shown in Table I.

All the cables have the same parameters. The fourth-order Runge–Kutta method solves the differential equation. According to the critical scale method and field commissioning, the control parameters $\boldsymbol{K}_{pp}$, $\boldsymbol{K}_{pd}$, $\boldsymbol{K}_{lp}$ and $\boldsymbol{K}_{ld}$ are determined.

The initial position of the end-effector is $\boldsymbol{X}_0 = \begin{bmatrix} R & 0 & 5 \end{bmatrix}^T$, and R is the helix radius. The initial running height of the cable-driven parallel camera robot is $Z_0 = 5m$. The trajectory is the spatial cylindrical spiral trajectory with the helix radius of $R_1 = 10$ m, $R_2 = 15$ m, $R_3 = 18$ m, $R_4 = 20$ m, respectively. This four helix radius correspond to four different line speeds. The run time is $t = 10$ s always, and the angular velocity is $\boldsymbol{\omega} = 0.2\pi$ rad/s always. The line speed in the XOY plane is $v_1 = \boldsymbol{\omega} R$. The speed in Z-direction is $\boldsymbol{v}_Z = 0.628$ m/s always. The resultant velocity is $\boldsymbol{v} = \sqrt{\boldsymbol{v}_1^2 + \boldsymbol{v}_Z^2}$. As shown in Fig. 7, the simulation trajectory is described by the following equation:

$$\begin{cases} \boldsymbol{x} = R\cos(\boldsymbol{\omega} t) \\ \boldsymbol{y} = R\sin(\boldsymbol{\omega} t) \\ \boldsymbol{z} = \boldsymbol{v}_Z t + 5 \end{cases} \tag{35}$$

6.2. Results and discussions

The changes of the cable lengths at different speeds are shown in Fig. 8. It can be seen from the figure that the cable lengths at different speeds are cyclical in the whole tracking process. The change of each cable is continuous and smooth, and there is no cable beating. These phenomena show that the control strategy is reasonable and can ensure the system operates normally. It is noteworthy from the figure that the changes of 1# cable length and 3# cable length are complementary at different speeds, since 1# cable and 3# cable have diagonal relationship. Similarly, 2# cable and 4# cable are the same. It can be seen from the figure that the greater the speed is, the greater the lengths of 1# cable and 4# cable are, and the shorter the lengths of 2# cable and 3# cable are. This is because of changing the running speed by changing the helix radius. That is to say, the greater the speed is, the greater the helix radius. Then the starting point $\boldsymbol{X}_0 = \begin{bmatrix} R & 0 & 5 \end{bmatrix}^T$ of the end-effector is close to 2# cable and 3# cable, so 2# cable length and 3# cable length are shorter, and 1# cable length and 4# cable length are longer. It is also known from the figure that the overall trend of the cable length is shorter and shorter as the end-effector moves higher and higher.

The changes of the cable tensions along the space spiral trajectory at different speeds are shown in Fig. 9. It can be seen from the figure that the cable tensions are smooth and continuous, which

https://doi.org/10.1017/S0263574719000201 Published online by Cambridge University Press

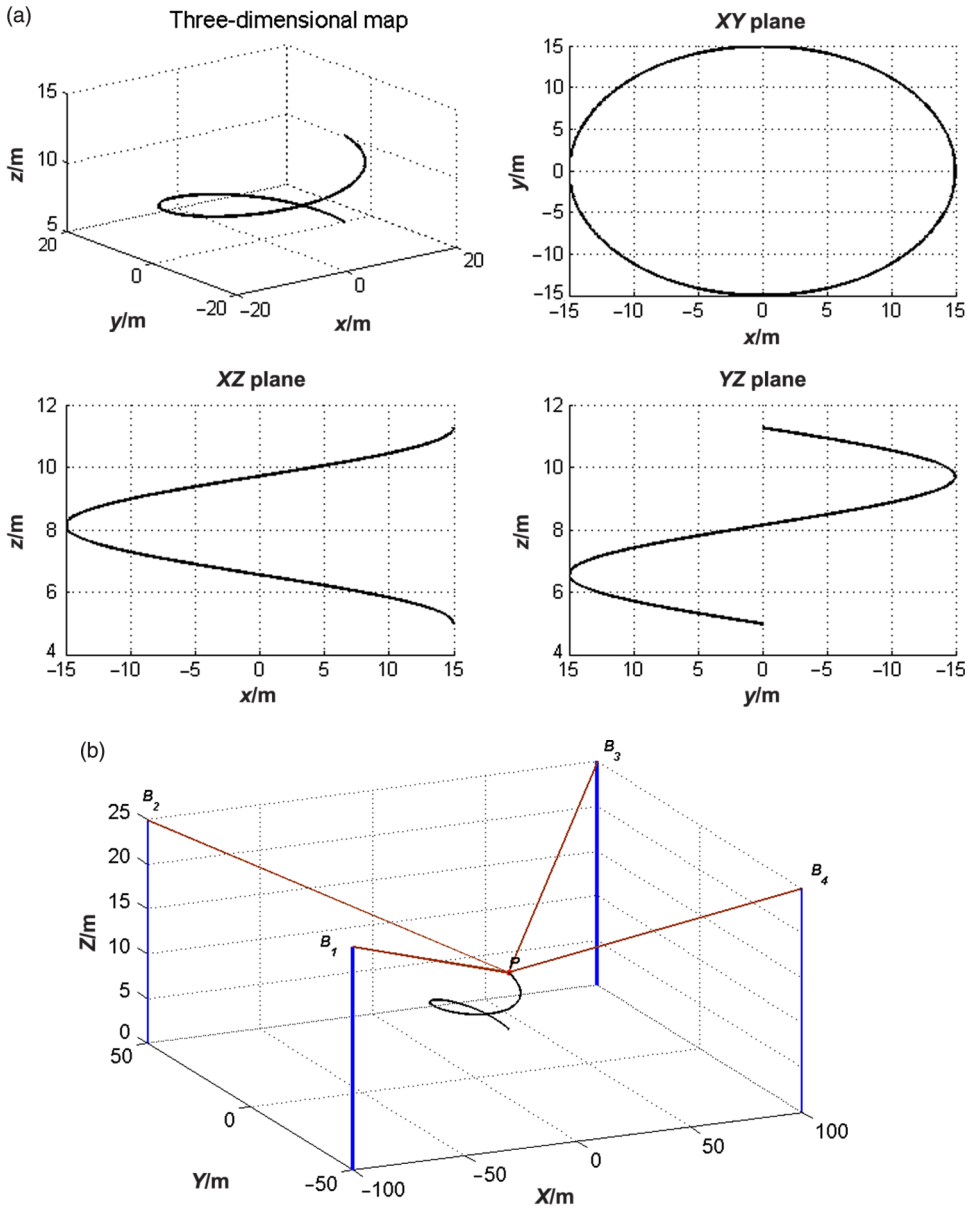

Fig. 7. The spatial cylindrical spiral trajectory: (a) trajectory in the *XYZ* plane; (b) space helix trajectory.

meets the expectation. The cable tensions increase with the increasing speed. This is because the radius of the helical path increases and the centripetal acceleration becomes larger, and the required centripetal force becomes larger, so the cable tensions become larger. With the increasing height of the end-effector, the cable tensions are also increasing, so the tension curve in Fig. 9 shows a tendency to rise periodically. When $\boldsymbol{v} = 6.31$ m/s, $m = 20$ kg, the site size is $39 \times 42 \times 25$ and the maximum actuation cable tension is 148 N; when $\boldsymbol{v} = 6.31$ m/s, $m = 20$ kg, the site size is $200 \times 100 \times 25$ and the maximum actuation cable tension is 302 N,[10] the cable tension increased by about two times, which indicates that the weight of the cable is not negligible in large-span system. Therefore, the catenary model is more accurate than the linear model in large-span system. When $\boldsymbol{v} = 9.44$ m/s, there was the cable pseudo-drag problem in the literature,[10] and the active synchronous cable tension controller is designed in this paper to effectively avoid the cable pseudo-drag problem. The cable tensions are smooth and continuous, and there is no cable pseudo-drag problem with the control strategy designed in this paper. It is proved that the active synchronous cable tension control can effectively avoid the cable pseudo-drag problem under high-speed motion.

https://doi.org/10.1017/S0263574719000201 Published online by Cambridge University Press

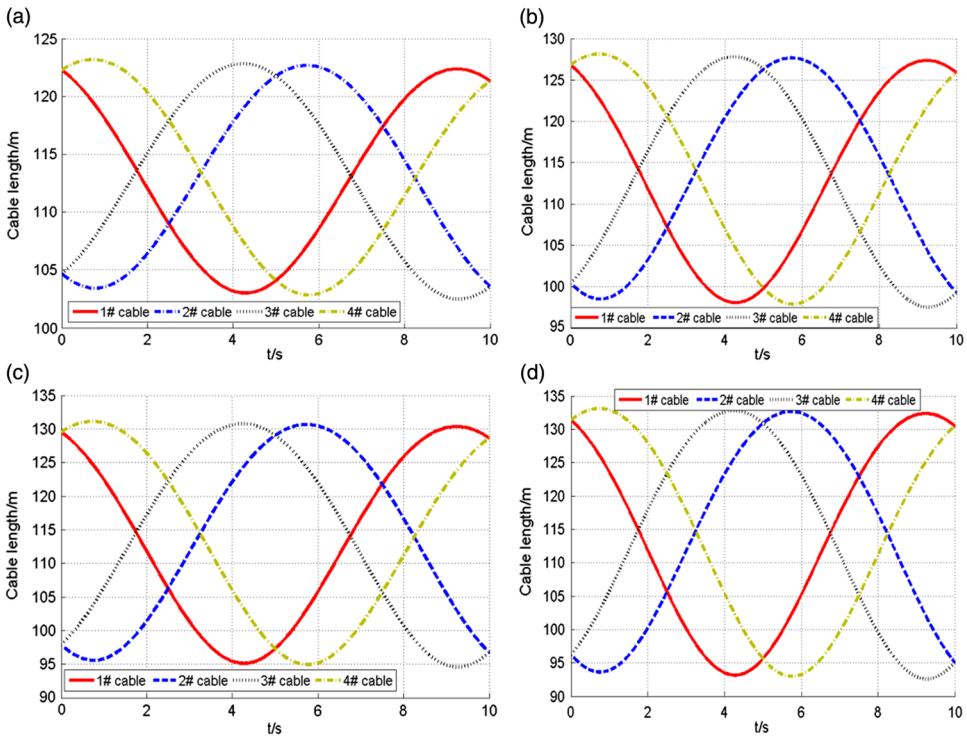

Fig. 8. Cable lengths at different speeds: (a) $v = 6.31$ m/s; (b) $v = 9.44$ m/s; (c) $v = 11.32$ m/s; (d) $v = 12.58$ m/s.

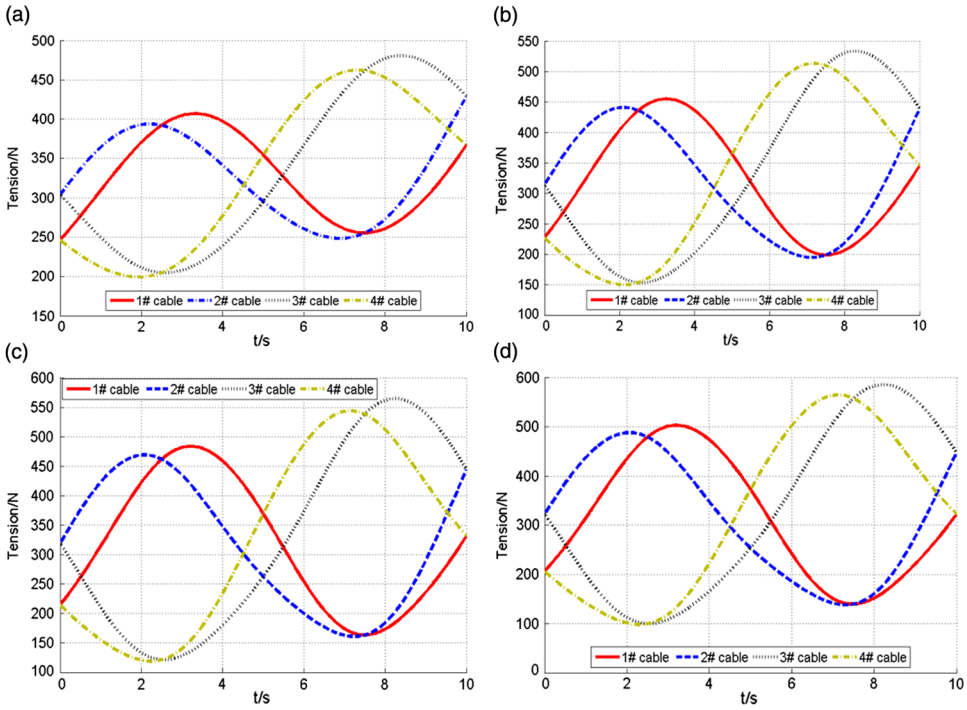

Fig. 9. Cable tensions at different speeds: (a) $v = 6.31$ m/s; (b) $v = 9.44$ m/s; (c) $v = 11.32$ m/s; (d) $v = 12.58$ m/s.

Figure 10 shows the position error of the end-effector under different control strategies. In order to illustrate the superiority of the hybrid control scheme, we compare the traditional PID (proportion, integral, differential) control, PD control, PD-modified feedforward control and hybrid position/tension control. As seen from the figure, the hybrid position/tension control has a higher

https://doi.org/10.1017/S0263574719000201 Published online by Cambridge University Press

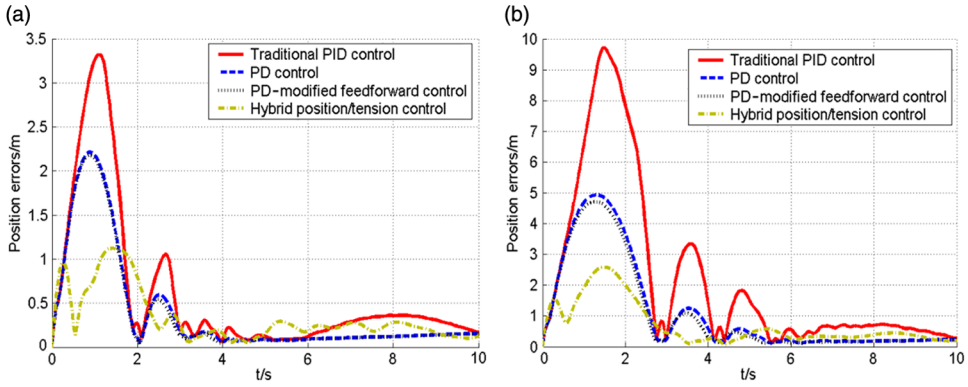

Fig. 10. Position errors under different control strategies: (a) $v = 6.31$ m/s; (b) $v = 9.44$ m/s.

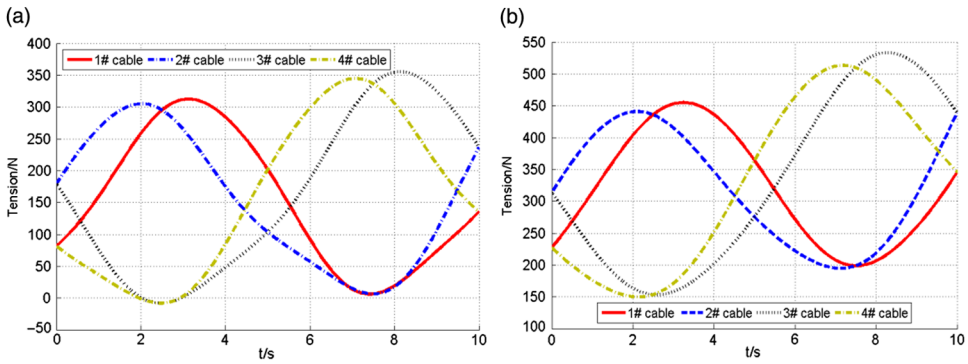

Fig. 11. Comparison of cable tensions at $v = 9.44$ m/s: (a) no active tension controller; (b) with active tension controller.

position tracking accuracy compared with other control methods with high-speed motions. During the start-up phase, the peak position errors using the hybrid position/tension control are 50% less than that using the PD-modified feedforward control.

Figure 11 shows a comparison of the cable tension when there is active synchronous cable tension control and when there is not while the end-effector operates at $v = 9.44$ m/s. Their movement trajectories are the same; both are the spatial cylindrical spiral trajectories. From Eqs. (19) and (20), we have $\boldsymbol{T}_i = \boldsymbol{V}_i \frac{\tan \gamma_i}{\sqrt{1+\tan^2 \gamma_i}}$. When $\boldsymbol{v}_i < 0$, the cable-driven parallel robots are in the pseudo-drag state. That is to say, when $\boldsymbol{T}_i < 0$, the cable-driven parallel robots are in the pseudo-drag state. It can be seen that there is the cable pseudo-drag when there is no active synchronous cable tension control. The cable tension is less than zero between 2 and 4 s. When there is active synchronous cable tension control, the cable pseudo-drag phenomenon disappears, and the minimum cable tensions are about 150 N as shown in Figure 11. That is to say, it is necessary to use the active synchronous cable tension control to avoid the cable pseudo-drag problem when the cable length adjustment is beyond the PD-modified feedforward control adjustment range.

7. Conclusions

This paper studies the cable pseudo-drag problem of the cable-driven parallel camera robots at high speeds. In order to solve the cable pseudo-drag problem, this paper introduces the active synchronous cable tension control based on PD-modified feedforward control method. It is a hybrid position/tension control which achieves the purpose of cable tension active control and avoids the cable pseudo-drag problem at high speeds. The catenary equation of the cable-driven parallel robot is established firstly and the critical condition of the cable pseudo-drag is determined. The system dynamic model is established according to the catenary equation, and the cable tensions are optimized according to the dynamic model. On the basis of the above work, a hybrid position/tension control strategy based on cable tension optimization is proposed. Then the stability and uniform continuity of the

https://doi.org/10.1017/S0263574719000201 Published online by Cambridge University Press

control strategy are proved by Lyapunov stability theory. The simulation results of high-speed cable-driven parallel camera robots show that the control method is effective and reasonable. Also, with the comparison of medium speed and high speed, it is shown that the hybrid position/tension control strategy based on cable tension optimization can effectively avoid the cable pseudo-drag problem.

Conflicts of Interest

The authors declare that there is no conflict of interest regarding the publication of this paper.

Acknowledgements

The authors gratefully acknowledge the financial support of the National Natural Science Foundation of China under Grant No. 51175397.

References

1. J. Albus, R. Bostelman and N. Dagalakis, "The NIST robocrane," *J. Rob. Syst.* **10**(5), 709–724 (1993).
2. H. L. Wei, Y. Y. Qiu and J. Yang, "An approach to evaluate stability for cable-based parallel camera robots with hybrid tension-stiffness properties," *Int. J. Adv. Rob. Syst.* **12**(185), 1–12 (2015).
3. C. B. Pham, G. L. Yang and S. H. Yeo, "Dynamic Analysis of Cable-driven Parallel Mechanisms," *Proceedings of the 2005 IEEE/ASME International Conference on Advanced Intelligent Mechatronics*, Monterey, California, USA (2005) pp. 612–617.
4. E. Ottaviano, M. Ceccarelli and P. Pelagalli, "A Performance Analysis of a 4 Cable-driven Parallel Manipulator," *Proceedings of the 2006 IEEE Conference on Robotics, Automation and Mechatronics*, Bangkok, Thailand (2006) pp. 1–6.
5. R. L. Williams II and P. Gallina, "Translational planar cable-direct-driven robots," *J. Rob. Syst.* **37**, 69–96 (2003).
6. W. L. Wang, X. Sun and B. Y. Duan, "Concept of parallel macro/micro manipulator and optimal scheme for cable tension in the FAST project," *J. Xidian Univ.* **6**(27), 726–729 (2000) (in Chinese).
7. X. Sun and B. Y. Duan, "Study on solution space, working space and cable tension's optimized analysis for huge flexible Stewart platform," *Chin. J. Mech. Eng.* **2**(38), 16–21 (2002) (in Chinese).
8. A. F. Tang, Y. Y. Qiu and B. Y. Duan, "Optimal structural design, pseudo-drag cable restriction analysis and experimental study of wind-induced vibration of a large radio telescope with an additional vessel," *Mech. Sci. Technol. Aerosp. Eng.* **5**(26), 610–614 (2007).
9. R. Yao, X. Q. Tang, J. S. Wang and P. Huang, "Dimensional optimization design of the four-cable driven parallel manipulator in FAST," *IEEE/ASME Trans. Mechatr.* **15**(6), 932–941 (2010).
10. X. Q. Tang and Z. F. Shao, "Trajectory generation and tracking control of a multi-level hybrid support manipulator in FAST," *Mechatronics* **23**, 1113–1122 (2013).
11. H. L. Wei, Y. Y. Qiu and Y. Su, "Motion control strategy and stability analysis for high speed cable-driven camera robots with cable inertia effects," *Int. J. Adv. Rob. Syst.* **13**, 1–14 (2016).
12. K. Kozak, Q. Zhou and J. S. Wang, "Static analysis of cable-driven manipulators with non-negligible cable mass," *IEEE Trans. Rob.* **22**(3), 325–433 (2006).
13. M. Irvine, *Cable Structures* (MIT Press, Cambridge, MA, 1981).
14. N. Riehl, M. Gouttefarde, S. Krut, C. Baradat and F. Pierrot, "Effects of Non-negligible Cable Mass on the Static Behavior of Large Workspace Cable-driven Parallel Mechanisms," *IEEE International Conference on Robotics and Automation (ICRA)*, Kobe, Japan (2009) pp. 2193–2198.
15. S. Z. Shen, C. B. Xu and C. Zhao, *Cable Structure Design* (China Architecture & Building Press, Beijing, 2006) (in Chinese).
16. Y. Su, Y. Y. Qiu and P. Liu, "The continuity and real-time performance of the cable tension determining for a suspend cable-driven parallel camera robot," *Adv. Rob.* **29**(12), 743–752 (2015).
17. R. L. Williams II, P. Gallina and J. Vadia, "Planar translational cable-direct-driven robots," *J. Rob. Syst.* **20**(3), 107–120 (2003).
18. R. Verhoeven, Analysis of the Workspace of Tendon-Based Stewart Platforms *Ph.D. Dissertation* (University of Duisburg-Essen, 2004).
19. F. L. Lewis, D. M. Dawson and C. T. Abdallah, *Robot Manipulator Control: Theory and Practice* (Marcel Dekker, New York, 2004).
20. A. Vafaei, M. M. Aref and H. D. Taghirad, "Integrated Controller for an Over-constrained Cable Driven Parallel Manipulator: KNTU CDRPM," *Proceedings of the IEEE International Conference on Robotics and Automation*, Alaska (2010) pp. 650–655.